



Towards deciphering the Cenozoic evolution of the East Pisco Basin (southern Peru)

C. Di Celma, P.P. Pierantoni, T. Volatili, G. Molli, S. Mazzoli, G. Sarti, S. Ciattoni, G. Bosio, E. Malinverno, A. Collareta, K. Gariboldi, A. Gioncada, D. Jablonska, W. Landini, M. Urbina & G. Bianucci

To cite this article: C. Di Celma, P.P. Pierantoni, T. Volatili, G. Molli, S. Mazzoli, G. Sarti, S. Ciattoni, G. Bosio, E. Malinverno, A. Collareta, K. Gariboldi, A. Gioncada, D. Jablonska, W. Landini, M. Urbina & G. Bianucci (2022) Towards deciphering the Cenozoic evolution of the East Pisco Basin (southern Peru), *Journal of Maps*, 18:2, 397-412, DOI: [10.1080/17445647.2022.2072780](https://doi.org/10.1080/17445647.2022.2072780)

To link to this article: <https://doi.org/10.1080/17445647.2022.2072780>



© 2022 The Author(s). Published by Informa UK Limited, trading as Taylor & Francis Group on behalf of Journal of Maps



[View supplementary material](#)



Published online: 07 May 2022.



[Submit your article to this journal](#)



Article views: 1313



[View related articles](#)



[View Crossmark data](#)



Citing articles: 4 [View citing articles](#)



Towards deciphering the Cenozoic evolution of the East Pisco Basin (southern Peru)

C. Di Celma ^a, P.P. Pierantoni ^a, T. Volatili ^a, G. Molli ^b, S. Mazzoli ^a, G. Sarti ^b, S. Ciattoni ^c, G. Bosio ^d, E. Malinverno ^d, A. Collareta ^b, K. Gariboldi ^b, A. Gioncada ^b, D. Jablonska ^a, W. Landini ^b, M. Urbina ^e and G. Bianucci ^b

^aScuola di Scienze e Tecnologie, Università di Camerino, Camerino, Italy; ^bDipartimento di Scienze della Terra, Università di Pisa, Pisa, Italy;

^cScuola di Scienze Geologiche e Ambientali, Università degli studi di Urbino, Urbino, Italy; ^dDipartimento di Scienze dell'Ambiente e della Terra, Università di Milano-Bicocca, Milano, Italy; ^eDepartamento de Paleontología de Vertebrados, Museo de Historia Natural-UNMSM, Lima, Peru

ABSTRACT

The Cenozoic succession of the East Pisco Basin preserves the sedimentary record of several episodes of deformation of the forearc crust along the Peruvian margin. The 1:50,000 scale geological map presented here encompasses an area of about 1,000 km² lying astride the Ica River, and contributes to our understanding of the timing and mode of basin filling and deformation. Our novel two-fold megasequence framework provides a sound basis for establishing a first-order tectono-stratigraphic setting of the mid-Eocene–upper Miocene succession exposed in the study area. We interpret that the mid-Eocene to lower Oligocene succession studied in this work (megasequence P) was deposited in a single forearc basin, which was dissected into the present-day West and East Pisco basins by a fault-bounded basement high during the late Oligocene, and subsequently overlain by the Miocene fill of the East Pisco basin (megasequence N).

ARTICLE HISTORY

Received 7 February 2022

Revised 29 March 2022

Accepted 27 April 2022

KEYWORDS

East Pisco Basin; basin inversion; forearc basin; Cenozoic

1. Introduction

Forearc basins develop as a manifestation of permanent deformation related to subduction processes along both accreting and non-accreting convergent margins (Noda, 2016). The stratigraphic patterns of their filling successions are constantly shaped by the interplay between various styles of structural deformation, spatial and temporal variations in subsidence and uplift, sediment flux, and eustatic sea-level changes (e.g. Andjić et al., 2018; Di Celma & Cantalamessa, 2007; McNeill et al., 2000). Several recent studies have shed light on some of the above topics (e.g. Hernández et al., 2020; Kent et al., 2020; Witt et al., 2019), but major gaps remain unanswered because of the lack of fully integrated stratigraphic and structural researches.

The East Pisco Basin (EPB) is a NW-SE elongated depression belonging to the Peruvian forearc system (Figure 1a) and, because of its excellent exposure, it is a natural laboratory for the study of the stratigraphic architecture and deformation of forearc basins. The basin fill contains middle Eocene to lower Pliocene sediments (e.g. Dunbar et al., 1990), which are widely known for their exceptionally preserved fossil assemblages (e.g. DeVries, 2016, 2019; Esperante et al., 2015; Bianucci et al., 2016a, b, c, 2018a, b; Gariboldi et al., 2015; Gioncada et al., 2016, 2018a, b; Stucchi

et al., 2016; Landini et al., 2017a, b, 2019; Marx et al., 2017a, b; Lambert et al., 2018, 2020, 2021; Bosio et al., 2021a, b; Collareta et al., 2021b; Sanfilippo et al., 2021; Kočí et al., 2021).

Despite the well-preserved nature of this forearc basin, there is still a dearth of detailed stratigraphic studies, and stratal correlations across significant distances are problematic and commonly hindered by the lack of adequate age control and limited knowledge of the stratigraphic architecture. Covering about 1,000 km² of the central EPB (Figure 1b), the 1:50,000 scale geological map (Main Map) presented here integrates unpublished and previously published (Di Celma et al., 2016a, b, 2017, 2018a, b, 2019; Collareta et al., 2021a) mapping investigations carried out by the authors. This map portrays the fine-scale subdivision of the basin fill and its stratigraphic architecture within the study area in unprecedented detail, extending significantly the previous geological knowledge based on less accurate mapping (e.g. León et al., 2008). The Main Map is complemented by a set of cross-sections summarizing structural and stratigraphic relationships and a N-S-oriented correlation panel created through correlation of key measured sections. The panel also summarizes unpublished and recently published biostratigraphic and

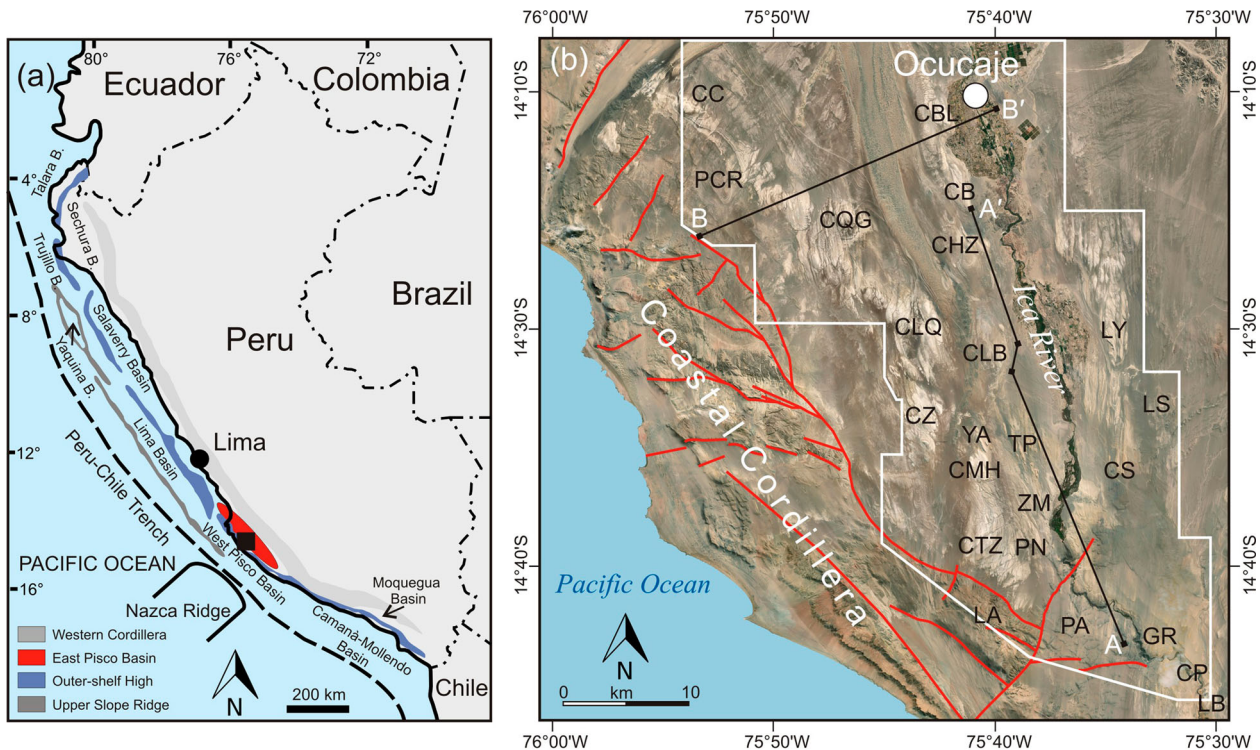


Figure 1. Location maps of the present study. (a) Sketch map of the major structural trends and basins of coastal Peru redrawn and modified from [Travis et al. \(1976\)](#) and [Thornburg and Kulm \(1981\)](#). The boxed area indicates the region of the EPB discussed in this paper. The black square shows position of (b) in the EPB; (b) annotated air photo showing location of the study area (outlined by a white frame), the NW-trending belt of uplifted basement rock along the southwestern side of the EPB known as the Outer Shelf High-Coastal Cordillera (red lines indicate main block-bounding normal faults), and localities mentioned throughout the text. The locality names are either official geographical names from the 1:100,000 scale base maps of Peru (sheets Lomitas 1741 and Ica 1742) or informal names assigned by [DeVries and Jud \(2018\)](#). Abbreviations: Cerro Colorado (CC), Pampa Concha Roja (PCR), Cerro Queso Grande (CQG), Cerro Ballena (CBL), Cerro Blanco (CB), Cerro Hueco la Zorra (HZ), Cerro la Bruja (CLB), Yesera de Amara (YA), Las Tres Piramides (TP), Cerro la Yesera (LY), Cadenas de los Zanjones (CZ), Cerro Mama y la Hija (CMH), Zamaca (ZM), Cerro Tiza (CTZ), Piedra Negra (PN), Lomas de Amara (LA), Pampa de la Averia (PA), Gramadal (GR), Canyon de los Perdidos (CP), Laguna Seca (LS), Cerro Sichuita (CS), Laberinto (LB). Black lines A-A' and B-B' are lines of geologic cross sections.

geochronological data, providing a robust chronostratigraphic allocation of the mid-Eocene to upper Miocene sedimentary units exposed in the study area. As such, this study represents a major step forward for intra-basinal correlation between scattered and geographically disparate sections and highlights the importance of integrated mapping, stratigraphic and structural analysis, and age constraints for understanding the Cenozoic tectono-sedimentary evolution of the EPB.

2. Geological setting

The Peruvian forearc basin system ([Figure 1a](#)) is an example of trench-parallel double forearc basins, in which seaward (slope) and landward (shelf) basins are separated from each other by the Outer Shelf High, a NW-trending structural culmination of the Precambrian-Paleozoic basement uplifted during the Neogene ([Kulm et al., 1982](#); [Thornburg & Kulm, 1981](#)). Subduction of normal oceanic lithosphere and the buoyant Nazca Ridge beneath the Peruvian forearc, as well as the southward migration of this latter during the past 16-11 Myr ([Hagen & Moberly, 1994](#);

[Hampel, 2002](#)), have produced several effects on the leading edge of the overriding plate. In particular, rapid convergence is interpreted as driving subduction erosion and subsidence of the forearc area ([Clift et al., 2003](#); [von Huene & Lallemand, 1990](#)), while slower rates of convergence were associated with its uplift and erosion. Major plate reorganization events were characterized by significant changes in rate and direction of plate convergence ([Herbozo et al., 2020](#)) and paralleled periods of Andean orogeny like the mid-Eocene Incaic II (43-42 Ma) and middle to late Oligocene Aymara (30-27 Ma) compressional phases ([Sébrier et al., 1988](#)). Nowadays, about 20% of the EPB lies offshore north of the city of Pisco, with the onshore portion being bounded to the northeast by the Western Cordillera and to the southwest by the Coastal Cordillera (the subaerial prolongation of the Outer Shelf High; [Romero et al., 2013](#)). According to [Viveen and Schlunegger \(2018\)](#), the EPB has experienced substantial subsidence for most of its Cenozoic history and its exhumation is interpreted as a manifestation of the Nazca Ridge subduction beneath this part of the Peruvian forearc during the Quaternary (e.g. [Hsu, 1992](#); [Macharé & Ortíeb, 1992](#)).

3. Regional stratigraphy

The rocks exposed within the study area can be broadly divided into: (i) basement sequence, comprising metamorphic rocks of the Proterozoic Arequipa Massif (Ramos, 2008), which are intruded by Paleozoic granites of the San Nicolás Batholith (Mukasa & Henry, 1990) and overlain by Jurassic volcaniclastic rocks of the Guaneros Formation; (ii) the middle Eocene-upper Miocene marine sedimentary succession summarized below; and (iii) Quaternary deposits, including gravel deposits interpreted as dissected alluvial fans, sediments filling of the modern Ica River valley, windblown sand, and rare primary gypsum deposits formed in small endorheic basins.

3.1. The middle Eocene-upper Miocene basin fill

Basement rocks are directly overlain by a middle Eocene-upper Miocene sedimentary succession with a maximum thickness of about 1 km (Figure 2). This sedimentary succession includes (from oldest to youngest): the Caballas, Paracas, Otuma, Chilcatay, and Pisco formations (DeVries, 2017; DeVries et al., 2017; DeVries & Jud, 2018; Dunbar et al., 1990). The Ypresian sedimentary rocks of the Caballas Formation (DeVries, 2017) cropping out in the northern and southern EPB, are not exposed in the study area. The boundaries of these lithostratigraphic units coincide with major regional unconformities of varying magnitude (DeVries, 1998). Consequently, these units should be regarded as alloformations, as defined by the NACSN (2005), or as depositional sequences in a genetic sense (Catuneanu et al., 2019), with each of them corresponding to either individual depositional sequences or groups of higher-order sequences (composite sequences) when punctuated by less pronounced unconformities. In this paper we have adopted the previously defined stratigraphic nomenclature, with names of the main unconformity-bounded sequences and composite sequences matching the traditionally employed formation names. Individual sequences and high-order sequences form the fundamental mapping units in this study; where the high-order unconformities were difficult to pick out with confidence, composite sequences were mapped as undifferentiated units. Individual and composite sequences stack to form two megasequences (megasequence P and N), which are bounded at the base by widespread unconformities reflecting major phases of basin evolution in response to regional tectonic events.

3.1.1. Megasequence P (Paleogene)

This megasequence, which is bounded at the base by the PaE0 unconformity (Figure 3a), encompasses the Paracas and Otuma sequences and rests

nonconformably on basement rocks. The PaE0 unconformity is commonly paved with basement-derived clasts in coarse-grained skeletal carbonate sand (Figure 3b). This basal conglomerate is followed by medium- to coarse-grained bioclastic sandstones (~20 m-thick) that grade upward into a monotonous succession of green-weathering siltstones (up to ~100 m-thick), representing deposition in shoreface and relatively deeper inner- to outer-shelf settings, respectively. Sedimentary rocks of the Paracas sequence were deposited during the late Lutetian (onset at ~43 Ma according to Coletti et al., 2019) to early Priabonian flooding of the basin (Lambert et al., 2017, 2019; Malinverno et al., 2021).

The overlying Otuma sequence is bounded at the base by the OE0 unconformity. This unit exceeds 290 m in total thickness and consists of a concretionary, fine- to medium-grained, ~10-m-thick sandstone package (Figure 3c) overlain by finely laminated siltstones. The basal sandstone package comprises two volcanic ash layers pointing to an age of ~37 Ma for the onset of the Otuma deposition (DeVries et al., 2017). Biostratigraphic data indicate that the Otuma strata exposed in the Zamaca area were deposited during the Priabonian (Malinverno et al., 2021). However, DeVries et al. (2017) report the occurrence of the early Oligocene diatom *Rouxia obesa* in samples from Cerro Tiza, suggesting that in the study area this sequence may include lower Oligocene strata.

3.1.2. Megasequence N (Neogene)

Sedimentary rocks of megasequence N, which comprise the Chilcatay and Pisco composite sequences, overlie megasequence P and, along the eastern margin of the basin, onlap onto the eroded basement. In the study area, the Chilcatay sequence is bounded at the base by the CE0.1 angular unconformity (Figure 4a, b). This sharp, erosional surface is commonly penetrated by a *Glossifungites* ichnofacies and includes branching systems of passively filled *Thalassinoides* burrows and, locally, clavate *Gastrochaenolites* borings (Figure 4c). CE0.1 is interpreted as recording a polygenic erosion surface due to amalgamation of subaerial erosion during sea-level lowstand and wave-cut planation during the subsequent transgression and widespread flooding of the basin.

In the study area, the Chilcatay composite sequence is composed of two high-order sequences (namely Ct1 and Ct2; Di Celma et al., 2019) separated by an internal unconformity (CE0.2). The ~50-m-thick Ct1 sequence comprises coarse-grained bioclastic sandstones interbedded with pebble to cobble conglomerates with clasts derived from the basement rocks that pass stratigraphically upward into thinly laminated siltstones with sand- and gravel-rich

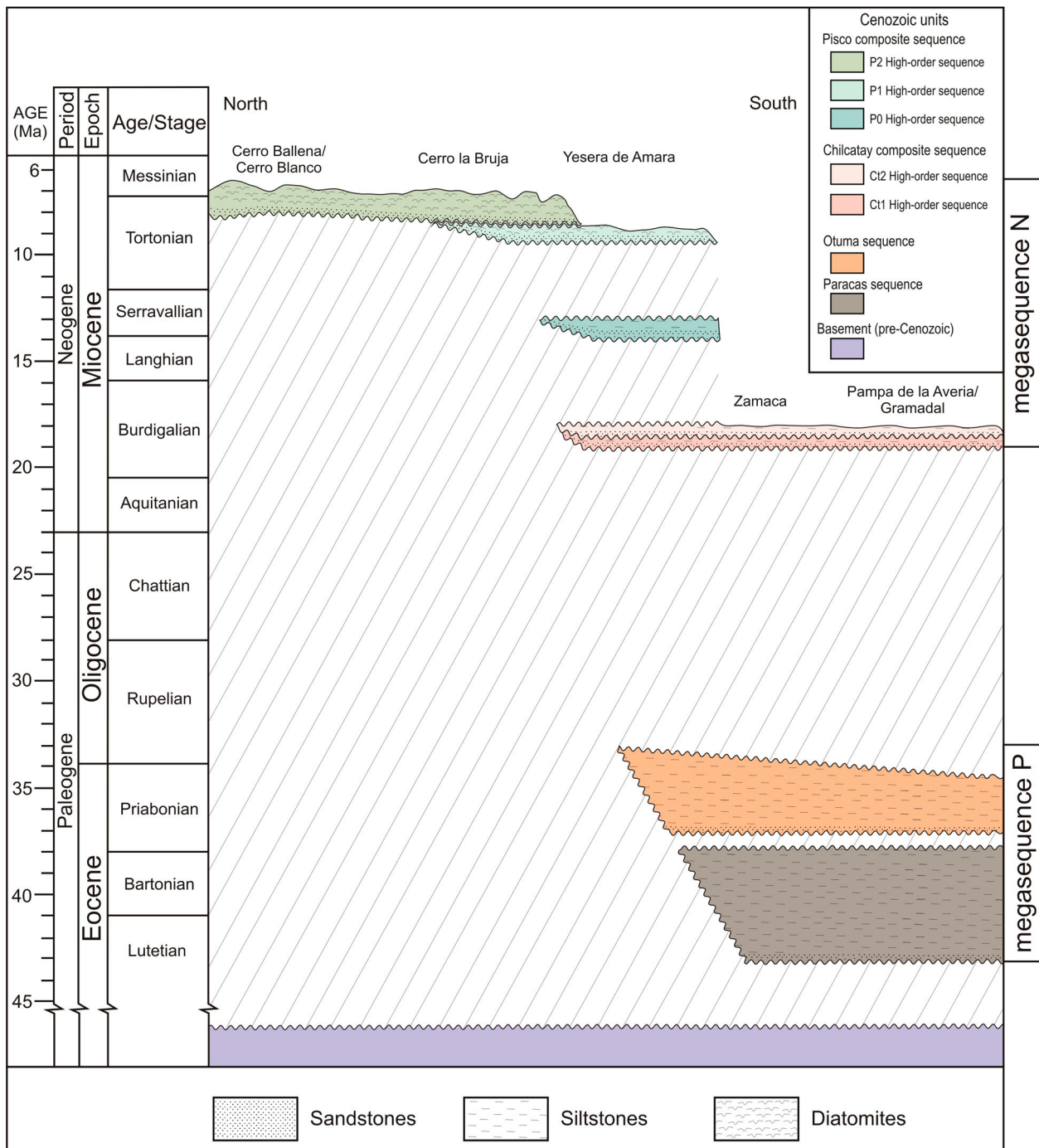


Figure 2. Roughly north (Cerro Ballena) to south (Pampa de la Averia) trending chronostratigraphic chart across the sedimentary fill of the EPB exposed along the Ica River valley. Note the occurrence of two megasequences (P and N) comprising two unconformity-bounded sequences (Paracas and Otuma) and two composite sequences (Chilcatay and Pisco), respectively. In turn, the Chilcatay and Pisco composite sequences include two (Ct1 and Ct2) and three (P0, P1, P2) high-order sequences, respectively. Hachured areas indicate major time gaps. The megasequence P unconformably overlies the underlying basement, and the megasequence N unconformably overlies the megasequence P with a certain time gap, indicating a tectonic event between deposition of the two stratal units.

intercalations and, ultimately, into a composite sediment wedge (Wright et al., 1989) interpreted a subaqueous marine delta (Hernández-Molina et al., 2000) prograding mainly from the northeast (Figure 4d). The ~20-m-thick Ct2 sequence is composed of a retrogradational shoreface to offshore succession comprising massive sandstones and thinly bedded siltstones, respectively. Between Zamaca, Cerro

Mama y la Hija, and Cerro Tiza, a distinctive sediment package comprised of intensely deformed strata is found intercalated with these undeformed strata and interpreted as the product of a submarine landslide (Figure 5a, b). Stratigraphic reconstructions indicate that its basal surface cuts at least 30 m down into the underlying sediments, incising the uppermost strata of Ct1 (Di Celma et al., 2019).

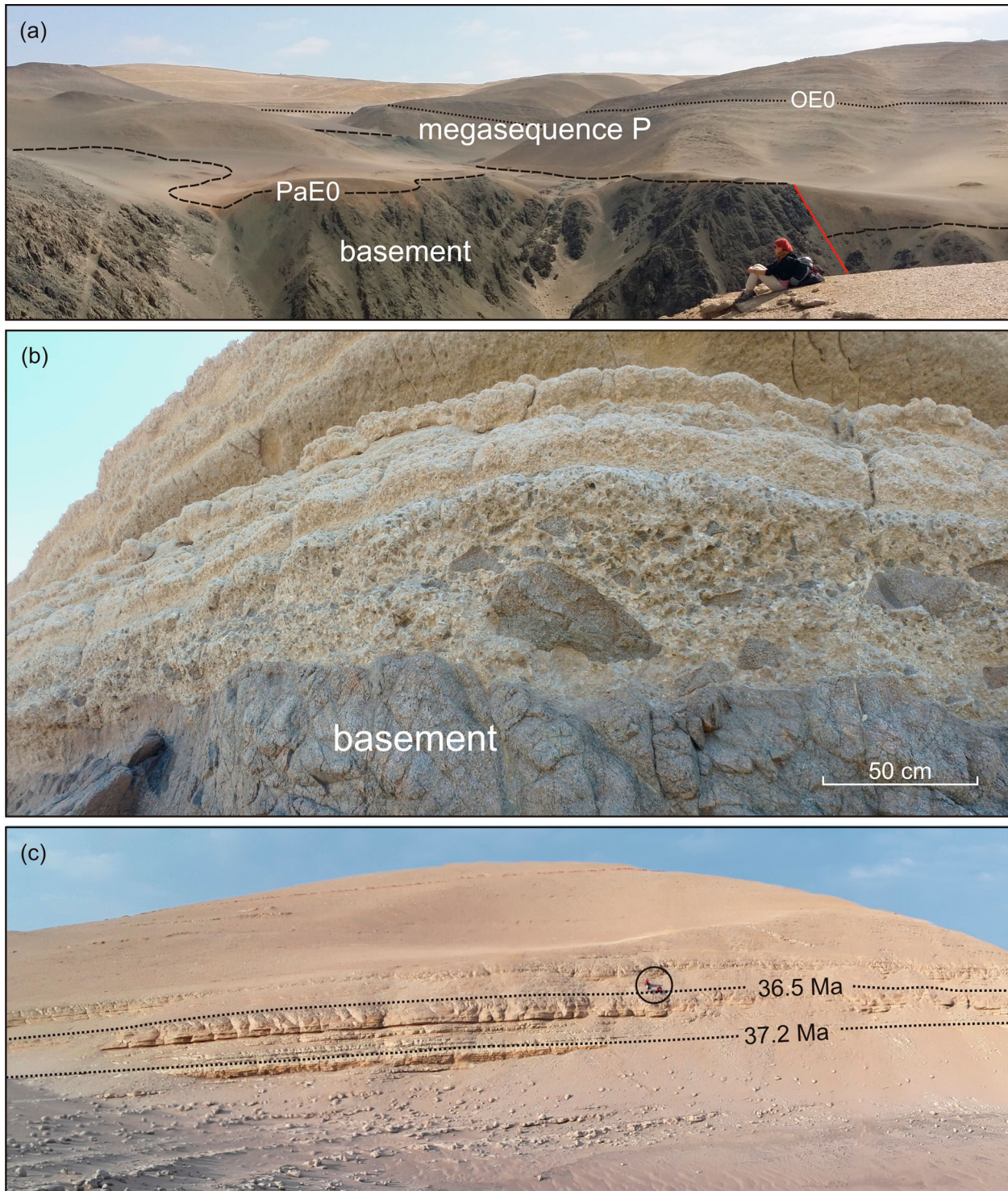


Figure 3. (a) Northeastward panoramic view of the megasequence P strata (Paracas and Otuma sequences) exposed along the eastward side of the Ica River valley at Pampa de la Averia; (b) outcrop detail of the basement-derived pebble- to cobble-sized clasts set in coarse-grained skeletal carbonate sand overlying the PaE.0 unconformity at the base of the Paracas sequence. The crystalline clasts mantling this surface are poorly rounded and have clearly not undergone significant transport. This transgressive lag was produced by wave reworking and winnowing of the underlying basement during relative sea-level rise and erosional shoreline retreat (Zecchin et al., 2018); (c) panoramic view of the base of the Otuma sequence at 14°39'42"S-75°37'5"W showing the basal concretionary sandstones and the position of two dated ash layers (dotted lines). Encircled geologists for scale.

Belia et al. (2019) analyzed nannofossil assemblages from exposures of the Ct2 sequence at Yesera de Amara and Las Tres Piramides and, based on the absence of *Discoaster druggii*, concluded that they are not younger than the earliest Miocene zone NN1 (~23 Ma). However, comprehensive micropaleontological studies

from Ct1 sediments exposed at Piedra Negra (Lambert et al., 2018) and Ct2 sediments exposed at Yesera de Amara (Di Celma et al., 2018b) indicate that rare specimens of *D. druggii* are already present in Ct1. This, along with silicoflagellate and diatom biostratigraphic markers, constrains the deposition of the Chilcatay strata

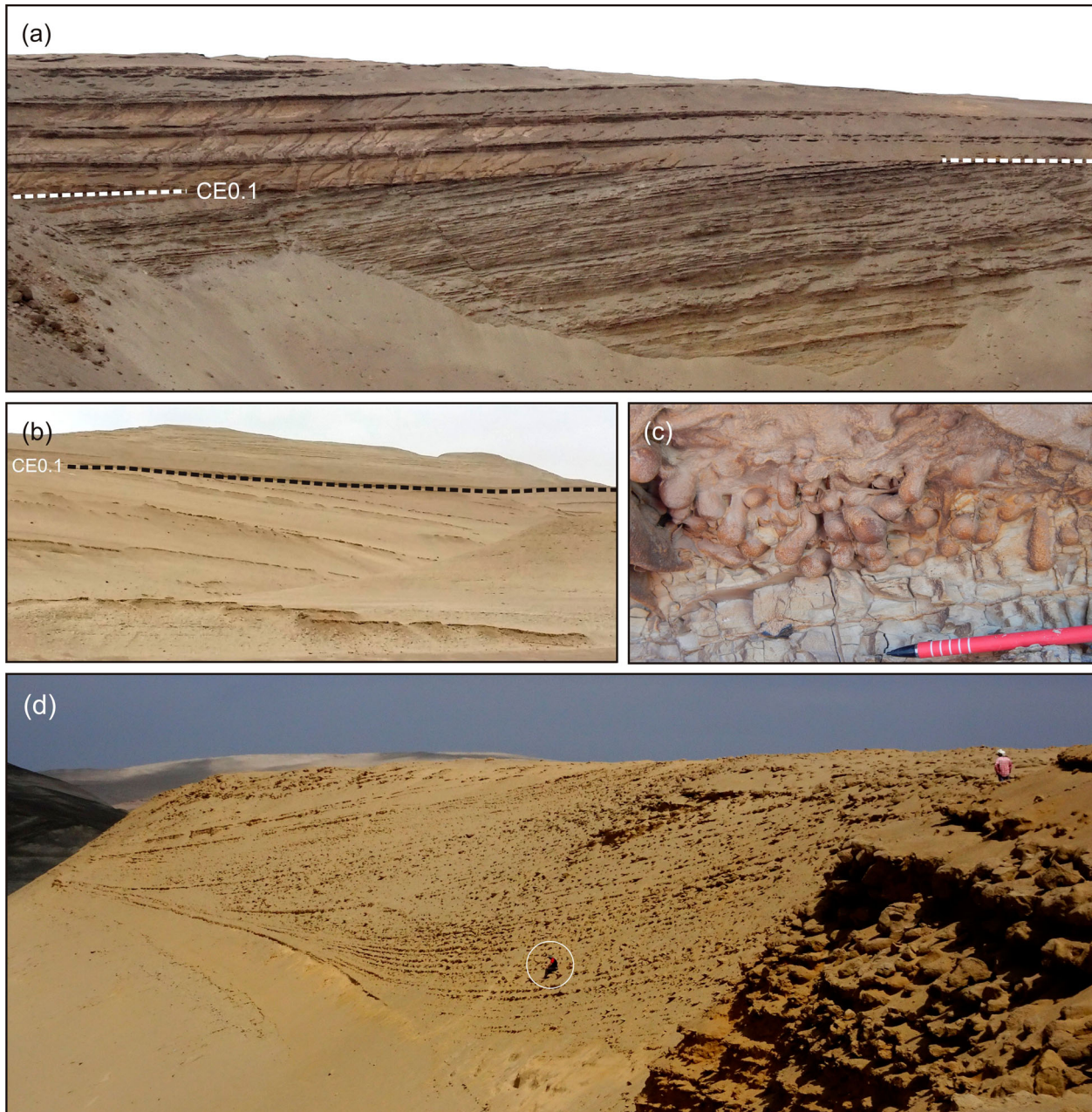


Figure 4. Panoramic views of the prominent CE0.1 angular unconformity at (a) Gramadal ($14^{\circ}42'16''S-75^{\circ}34'53''W$) and (b) Zamaca ($14^{\circ}39'15''S - 75^{\circ}38'25''W$); (c) oblique close-up photo of the CE0.1 *Glossifungites*-demarcated surface at Gramadal ($14^{\circ}41'56''S-75^{\circ}35'25''W$) showing vertical and oblique *Gastrochaeonolites* borings, interpreted as dwelling structures of bivalves, subtending from the surface and filled with sand penetrating from the overlying transgressive deposits. Together with *Gastrochaeonolites*, *Thalassinoides* are typical components of the firmground association analyzed along the CE0.1 unconformity, which indicates that construction of burrows occurred in a firm, compacted, but unlithified substrate (Carmona et al., 2007) and that the substrate-controlled ichnofacies demarcates a transgressively modified sequence-bounding discontinuity (e.g. MacEachern et al., 1992; Pemberton et al., 2004) characterized by lateral changes in the degree of substrate consistency; (d) panoramic view of the prograding wedge in the upper part of Ct1 at Canyon de los Perdidos ($14^{\circ}45'27''S-75^{\circ}30'48''W$). It is comprised of sets of delta-scale subaqueous clinoforms (*sensu* Patruno & Helland Hansen, 2018) that are tens of meters high and exhibit well-developed, flat to low-gradient topsets transitioning to steeper foresets and, ultimately, tangential bottomsets. Geologist (circled) for scale.

exposed in the study area between \sim 19–18 Ma. This younger age assignment of the Chilcatay strata is in excellent agreement with $^{87}\text{Sr}/^{86}\text{Sr}$ ages obtained from multiple samples from Ct1 (Bosio et al., 2020b) and $^{40}\text{Ar}/^{39}\text{Ar}$ biotite dating of three distinct volcanic ash layers collected near the base of Ct1 (19.25 ± 0.05 Ma), its middle portion (19.00 ± 0.28 Ma), and near the top of Ct2 (18.02 ± 0.07 Ma) (Bosio et al., 2020c;

Di Celma et al., 2018b). However, in a recent study undertaken at Laberinto, a locality just outside our study area, DeVries et al. (2021) documented an older unconformity-bounded unit (designated Chilcatay-0, or Ct0, by the authors) spanning the earliest Miocene between 21 Ma and \sim 19.8 Ma, which supports the interpretation that the lower portion of the Chilcatay composite sequence is largely diachronous across the



Figure 5. (a) Air photo image from Google Earth showing the NNW-trending eastern margin (dotted line) of the Ct2 submarine landslide in the Zamaca area and its jumbled up, chaotic internal nature. This chaotic sediment wedge, resulting from a major episode of instability and submarine mass-wasting, crops out over a 15 km^2 area and passes into the subcrop to the west, so that the western margin is not exposed; (b) westwards view of the mostly flat and horizontal base of the submarine landslide (marked by the dotted line) overlain by remobilized deposits dipping at high angles and locally overturned ($14^\circ37'52''\text{S}$ – $75^\circ38'36''\text{W}$). Encircled geologist for scale.

basin. Here, we propose that the three unconformities bounding the Ct0, Ct1 and Ct2 high-order sequences (CE0.0, CE0.1 and CE0.2) coalesce landward into a major one, which is designated CE0 and defines the base of the Chilcatay composite sequence. According to this hypothesis, Ct0 is the first sequence to pinch out by onlap outside the study area, causing CE0.0 and CE0.1 to merge. Within the study area, owing to the apparent absence of Ct0 strata, the temporal gap at the CE0.1 unconformity seemingly embraces the earliest Oligocene–early Miocene time interval (i.e. ~ 32 – 19 Ma). At a more basin-wide scale, however, the age of the CE0 unconformity can be bracketed between the youngest known strata of the Otuma sequence (earliest Oligocene) and the oldest known strata of the Chilcatay composite sequence (earliest Miocene), i.e. ~ 32 – 21 Ma.

The Chilcatay beds are separated from the overlying Pisco composite sequence by an angular unconformity. In the study area, the Pisco composite sequence attains a cumulative thickness of ~ 560 m (DeVries, 1998; DeVries & Jud, 2018; Dunbar et al., 1990). Stratigraphic analyses of the Pisco sediments exposed in the study area revealed multiple internal stratal surfaces, namely PE0.0, PE0.1, and PE0.2, which led to the identification and mapping of three unconformity-bounded, high-order sequences (Figure 6a), designated as P0, P1 and P2 in ascending stratigraphic order (Di Celma et al., 2016a, b; 2017, 2018a), preserved in an overall landward-stepping pattern. These surfaces display limited erosional relief and are interpreted as polygenetic surfaces formed by subaerial erosion during sea-level lowstand and subsequently modified by erosional transgression

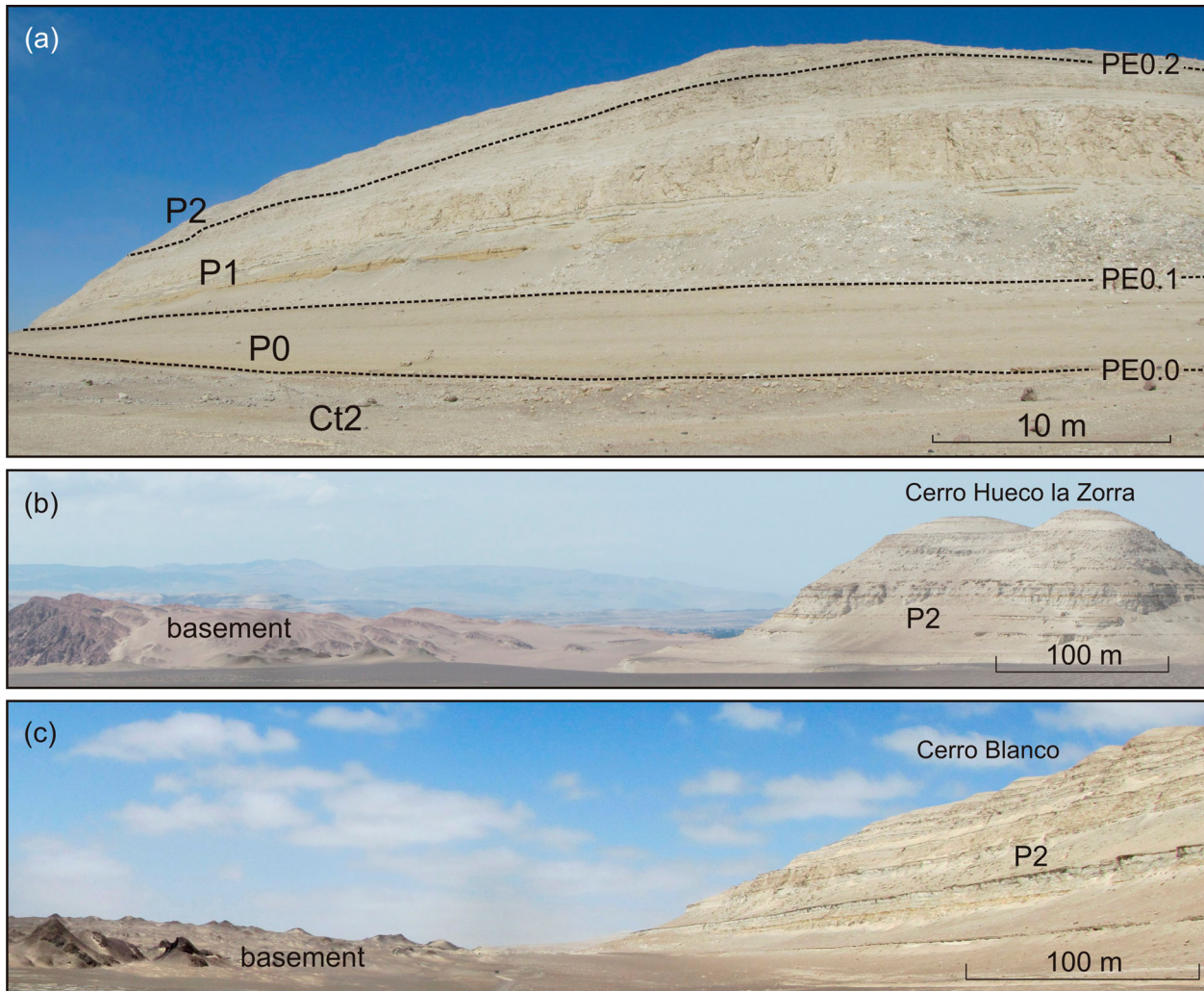


Figure 6. (a) Oblique field photograph of the western side of Cerro Mama y la Hija (approximately $14^{\circ}36'11''S - 75^{\circ}40'32''W$) showing high-order sequences (P0, P1, and P2) and interpreted sequence boundaries (PE0.0, PE0.1, and PE0.2) inside the Pisco composite sequence; (b) southward panoramic view of Cerro Hueco la Zorra and (c) southward panoramic view of Cerro Blanco showing upper Miocene P2 strata onlapping and wrapping around the crest of a basement topographic high.

during ensuing relative sea-level rise. They are typically overlain by thin conglomerate lags, comprising well-rounded, pebble-size phosphate nodules, mollusk shells, sparse polished vertebrate bones and teeth, and subangular to rounded crystalline cobbles and boulders, which grade upward into shoreface sandstones and overlying finer-grained, diatom-rich offshore deposits recording continuous transgression. Northeastward, PE0.0, PE0.1, and PE0.2 merge to form a composite, diachronous basal unconformity (PE0) formed during successive sea-level encroachments and planation episodes.

Strontium isotope-ratio ($^{87}\text{Sr}/^{86}\text{Sr}$) dating on shark teeth, mollusks and barnacles indicates that in the study area deposition of P0 occurred between 14.8 and 12.4 Ma (Bosio et al., 2020b). In agreement with these results, DeVries et al. (2021) constrained the age of a P0-equivalent strata exposed at Laberinto between 13.9–13 Ma by using diatom biostratigraphy. Diatom biostratigraphy of P1 and P2 sediments exposed at Cerro Colorado, Cerro los Quesos and

Cadenas de los Zanjones, and numerous $^{40}\text{Ar}/^{39}\text{Ar}$ age determinations on interbedded tephra layers give mutually consistent results and concur in indicating their deposition between 9.5 and 8.6 Ma, and 8.4 and ≥ 6.71 Ma, respectively (Bosio et al., 2020c; Gariboldi et al., 2017). In addition, the diatom species *Lithodesmium reynoldsii* (9.9–8.9 Ma) and *Denticulopsis praekatayamae* (9.5–8.5 Ma) occur throughout the entire sections of P1 strata exposed at Cerro Mama y la Hija and at Cerro Tiza, further supporting (in contrast to previous interpretations by DeVries et al., 2021) the 9.5 Ma age assignment for the oldest P1 rocks exposed west of the Ica River.

Owing to a persistent landward onlap onto a gently sloping surface on lower Miocene strata and basement rocks, the Pisco composite sequence thins rapidly northeastward. Between Cerro Hueco la Zorra and Cerro Blanco, P2 strata onlap and wrap around a basement high, which is consistent with marine transgression onto the flanks of a basement paleo-island that was flooded and completely submerged during the

P2 transgression (Figure 6b, c). Based on radiometric dating of the intercalated ash layers, the youngest P2 strata exposed at Cerro Blanco are about 7.1 Ma old. Chemical and petrographic fingerprinting of tephra layers (Bosio et al., 2019, 2020a, c) and lateral tracing of lithological marker beds (Brand et al., 2011; Di Celma et al., 2017, 2018b) allow for long-distance correlations of this sediment package, from Cerro Blanco to the north through Cerro Hueco la Zorra, Cerro la Bruja, Cerro los Quesos, Cadenas de los Zanjones to Cerro Mama y la Hija to the south.

4. Structural overview

The southwestern margin of the EPB is defined by several fault-bounded basement highs forming the Outer Shelf High-Coastal Cordillera (Figure 1b). The basin fill is mildly deformed by multiple generations of variably striking faults, indicating a prolonged tectonic history, yet their age constraints, geometry and kinematic evolution remain uncertain. Rustichelli et al. (2016a, b) and Viveen and Schlunegger (2018) were the first to study these structures in detail. Based on an integrated study of satellite images and structural field-based mapping, Viveen and Schlunegger (2018) highlighted that three main sets of large, regional scale faults and lineaments are recognizable in the EPB, striking approximately 160°, 120° and 30°N. Our field survey reveals the occurrence of dominantly NW-striking and subordinate NE-striking faults dissecting the entire Eocene to Miocene succession, while prevalently ENE-striking and subordinately NNW-striking faults only affect the Eocene strata (Figure 7a, b). Rare kinematic indicators, such as slickenlines and/or slickenfibres, indicate dominant dip-slip extensional faulting for both the dominant NW- and ENE-striking sets.

The A-A' cross-section that accompanies the geological map of this study summarizes the structural and stratigraphic relationships in the area between Pampa de la Averia to the south and Cerro Blanco to the north. In the southern sector of the map, basement rocks are exposed at the surface or underpins outliers of the overlying Eocene sedimentary cover. Here, beds display a range of orientations, with prevalent dips of 10–20° towards the northeast, and both basement and overlying sedimentary cover are affected by NNW- and ENE-striking extensional faults showing maximum throw values around 40 m. Most of these normal faults do not affect the Miocene strata indicating that extensional faulting of the Eocene strata predated the development of the CE0.1 unconformity. However, some faults continued to be active, or were reactivated, during the early Miocene, as documented by markedly different offsets recorded by Eocene and Miocene markers that pre- and postdate the CE0 unconformity, respectively. Between

Zamaca and Cerro la Bruja, only rocks of megasequence N are exposed, with the Chilcatay strata revealing a range of bedding attitudes, and the Pisco beds dipping nearly uniformly 5–10° towards the northeast. However, ~5 km east of these localities, Eocene strata of the Paracas and Otuma sequences are exposed along both sides of the Ica River. In this portion of the map, the basin fill is dissected by numerous NW- to NNW-striking normal faults showing throws of less than 10 m and maximum lengths of 4 km (Figure 7b). Although the timing of these structures is difficult to constrain, in the mapped area they postdate the deposition of the Tortonian-Messinian P2 strata and predate the Pleistocene gravels of the Cañete Formation, which are seemingly not offset.

At Pampa Concha Roja, at the northwestern reaches of the mapping area, the oldest tectonic structures documented are NW-striking, SW- and NE-dipping normal faults juxtaposing basement rocks at the footwall against northeastward-dipping strata of megasequence P (to the west) and N (to the east). The resulting basement culminations are fringed by oyster-rich Chilcatay strata (DeVries & Jud, 2018) that were deposited while these structural highs formed islands protruding from the Paleogene basin fill sediments (Gran Tablazo Archipelago *sensu* DeVries & Jud, 2018). Farther east, between the basement culmination and Cerro Ballena (B-B' cross-section), bedding orientations of Chilcatay and Pisco strata generally record landward tilting by 10°–12°. They are preserved in a general landward-stepping stacking pattern with the progressive onlap on top of the basement towards the northeastern side of the basin recording progressive landward shift of deposition.

In the Pampa Concha Roja area, a second set of major intrabasinal structures is represented by NE-striking, steeply SE-dipping normal faults (Figure 7c, d) displaying narrow, fault-parallel anticlines in the immediate hanging-wall and little evidence of deformation of the footwall strata. A set of high-angle, NNW- to NNE-striking secondary faults having vertical offsets and lengths of less than 10 m and 0.6 km, respectively, clearly dissects and postdates both the older NE-trending faults and related fault-parallel hanging-wall anticlines. Rustichelli et al. (2016b) proposed that the NE-striking faults are oblique-slip structures with dominant dextral strike-slip components and minor normal dip-slip components. However, further detailed structural and kinematic analyses suggest that the narrow anticlines in the immediate hanging-wall of the NE-trending faults are inversion-related folds that developed by the oblique-slip reactivation of pre-existing normal faults (e.g. Phillips et al., 2020). The amount of shortening was small and insufficient to completely reverse the original extensional offset, with faults displaying net extensional displacements.

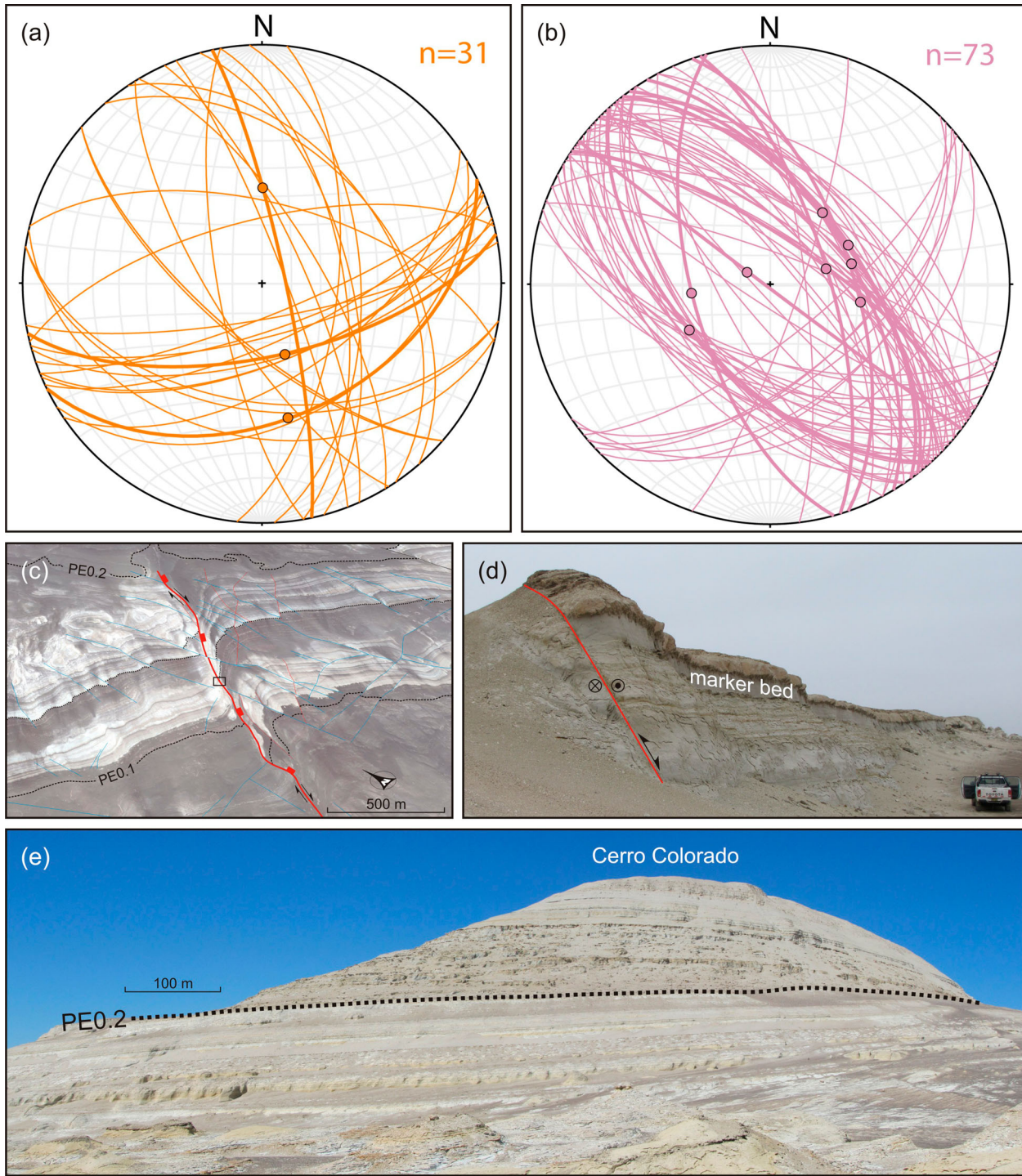


Figure 7. (a, b) Lower-hemisphere, equal-area projections of faults (great circles) and associated slip vectors (dots; recorded by striae and/or mineral fibres on fault surfaces) of the Eocene-Oligocene (orange) and Miocene (purple) successions measured at Gramadal (a), and Cerro de Los Zanjones, Cerro Mama y la Hija, Ullujaya and Cerro Colorado (b). Stereographic projections were made using Stereonet v. 11 software by Richard W. Allmendinger; (c) three-dimensional oblique aerial view from Google Earth of a spectacularly exposed fault-parallel, NE-plunging anticline in the immediate hanging-wall of a NE-trending, SE-dipping main fault (thick red line; squares give dip direction). The hanging-wall anticline incorporates lower to upper Miocene strata (Chilcatay and P1) before it is truncated upwards by the PE0.2 unconformity. The fold is dissected by secondary faults (thin red lines) that strike parallel and probably connect downwards to the adjacent main fault. A set of NNW- to NNE-striking normal faults (blue lines) offset and postdates the NE-striking fault and related hanging-wall anticline and secondary faults. The black dotted line and the black rectangle indicate a sandstone marker bed and position of photograph shown in (c), respectively; (d) field photograph looking northwards along the NE-trending fault shown in (c) ($14^{\circ}22'11''S$ – $75^{\circ}52'42''W$). Fault dips 65° SE and displays apparent normal-type displacement. The sandstone marker bed is indicated; (e) southeastwards view of P1 and P2 strata at Cerro Colorado (approximately $14^{\circ}20'48''S$ - $75^{\circ}53'56''W$). Bedding dips progressively decrease up-section indicating deposition of the upper Miocene strata during a period of syndepositional uplift and tilting. This fanning-dip geometry can be confidently related to the uplift of the fault-bounded basement high at the south-western margin of the EPB and landward tilting of the Miocene strata.

At Cerro Colorado, P1 and P2 strata show progressive up-section decrease in northeastward bedding dip (Figure 7e; Di Celma et al., 2016b). Their divergence away from the southwestern margin of the basin indicates a stratigraphic response to syndepositional uplift and tilting, thereby placing some constraints on the timing of the deformation.

5. Discussion and conclusions

In the study area, deposition initiated onto the PaE0 unconformity during the middle Eocene time, between 43.6 and 42.4 Ma, and continued under an extensional regime until late Eocene or early Oligocene time, with a break in deposition recorded by the OE0 unconformity separating the Paracas and Otuma sequences. During this time interval, a single forearc Pisco basin extended between an offshore outer forearc high and the Western Cordillera. In the Trujillo Basin (Figure 1a), the middle Eocene erosional unconformity truncating the crystalline basement is dated between 46–40 Ma (Prudhomme et al., 2019) and, therefore, it is largely equivalent to the PaE0 unconformity documented herein. According to Prudhomme et al. (2019), the middle Eocene subsidence of the forearc and landward shift of the Peruvian coastline took place as a result of relaxation and extension in the overriding plate following the Incaic II compressional event and a coeval increase in subduction erosion (Herbozo et al., 2020). An Oligocene relative sea-level fall, probably resulting from a combination of tectonic inversion and multiple events of eustatic lowstand, led the Pisco Basin to become subaerially exposed. Evidence for this phase of deformation is recorded by the conspicuous CE0.1 angular unconformity interposed between megasequences P and N. The oldest normal fault populations documented here consist of NNW- and ENE-trending faults largely predating the earliest Miocene CE0.1 erosional hiatus. This widespread extensional faulting was accompanied by the exhumation and subaerial exposure of major, fault-bounded basement highs forming the Outer Shelf High-Coastal Cordillera, which segmented the earlier, Paleogene Pisco Basin into the present-day inner (shelf) EPB and outer (slope) West Pisco Basin. Northwest and southeast of the Pisco Basin, respectively, the extensional Trujillo-Salaverry and Camaná-Mollendo basins were partially inverted during the Oligocene, resulting in the uplift of the Outer Shelf High and formation of a widespread Oligocene unconformity broadly synchronous with the early Oligocene-earliest Miocene CE0 unconformity (Alván et al., 2017; Genge et al., 2020; Prudhomme et al., 2019; Timoteo et al., 2017). These findings indicate that net uplift of the Peruvian forearc domain during the Oligocene was a regional phenomenon and that in the Pisco Basin it occurred despite active extension. Different tectonic processes have been invoked to explain the

Oligocene uplift of the extensional Peruvian forearc basins and formation of the Outer Shelf High, including crustal thickening by underplating at an erosive margin (Clift & Hartley, 2007; Draut & Clift, 2013) or inversion by propagation of basement-rooted, west-verging thrust faults (Quispe et al., 2018; Prudhomme et al., 2019; Ochoa et al., 2021). Thus, the EPB developed on the CE0 erosional surface and the bipartite arrangement of the basin fill succession described here is the most visible expression of the Oligocene regional change in basin configuration.

By earliest Miocene time uplift ceased, and subduction erosion and thinning of the overriding plate resulted in renewed subsidence, rise in relative sea level, and marine transgression over the CE0 unconformity. This regional transgression initiated with the deposition of the earliest Miocene Ct0 sediment wedge outside the study area and progressed with deposition of Ct1 and Ct2 inside the study area. Meanwhile, the basement structural highs occurring across the area (including inside the EPB and along its southwestern margin) formed a coastal archipelago (DeVries & Schrader, 1997).

Based on the deformation patterns outlined above, the early Miocene phase of extension and associated subsidence was followed by a late Miocene contractional tectonic event, with shortening being accommodated by: (i) oblique-slip (reverse plus dextral) reactivation of inherited NE-trending extensional faults, and development of associated fault-parallel hanging-wall anticlines; and (ii) renewal tectonic uplift of the southwestern basin margin resulting from the uplift of the seaward structural highs, as suggested by the fanning geometry of the northeast-dipping P1 and P2 strata exposed at Cerro Colorado and the landward shift of deposition, with progressive onlap of Pisco strata on top of the basement towards the northeastern side of the basin. The landward tilting of the upper Miocene strata may be ascribed to resumed uplift of the structural highs along the southwestern flank of the EPB during the Plio-Pleistocene. Similar tectonostratigraphic evolution and architectural style have been documented in roughly coeval strata elsewhere in the Peruvian forearc system through interpretations of seismic lines (Genge et al., 2020).

Software

The geological map was compiled by scanning hand drafts as black and white TIF files, and then digitizing the line art using the Corel Draw X3 graphics package. We used the GIS Data processing application Global Mapper 12 to generate contour lines for the 1:50,000 scale topographic base map. To do so, we relied on the digital elevation model (DEM) based on the Shuttle Radar Topography Mission 26 (SRTM), as released

by the United States Geological Survey (SRTM3 USGS version 2.1).

Data availability statement

The authors confirm that the field data supporting the findings of this study are available within the article and its supplementary material.

Acknowledgments

Our gratitude to Christian de Muizon, Olivier Lambert, Rodolfo Salas-Gismondi, Igor Villa, Rafael M. Varas-Malca, Thomas J. DeVries, Giovanni Coletti, Walter Aguirre, for their support, as well as for much fruitful discussions on the geology and paleontology of the East Pisco Basin. Journal reviewers Heike Apps, Michelangelo Martini, Simone Fabbi and Associate Editor Claudio Piccolomini are gratefully acknowledged for their thoughtful contribution and helpful criticism that sharpened the focus of this study.

Disclosure statement

No potential conflict of interest was reported by the author(s).

Funding

This work summarizes some of the results stemming from the multi-year study in the East Pisco Basin. Over these years, research was supported by grants from the Italian Ministero dell'Istruzione, dell'Università e della Ricerca (MIUR) to Bianucci (PRIN 2012 Project, 2012YJSBMK EAR- 9317031), Malinverno (PRIN Project, 2012YJSBMK_002), Di Celma (PRIN Project, 2012YJSBMK 003; FFABR 2017 grant); National Geographic Society Committee for Research Exploration to Bianucci (grant number 9410-13); the University of Pisa to Bianucci (PRA_2017_0032); the University of Camerino to Di Celma (FAR 2019 grant). FAR- University of Camerino

ORCID

- C. Di Celma  <http://orcid.org/0000-0001-7781-7981>
- P.P. Pierantoni  <http://orcid.org/0000-0002-1237-4689>
- T. Volatili  <http://orcid.org/0000-0001-9177-5706>
- G. Molli  <http://orcid.org/0000-0001-9488-8132>
- S. Mazzoli  <http://orcid.org/0000-0003-3911-9183>
- G. Sarti  <http://orcid.org/0000-0002-6327-4768>
- S. Ciattoni  <http://orcid.org/0000-0001-5342-5086>
- G. Bosio  <http://orcid.org/0000-0001-8067-4926>
- E. Malinverno  <http://orcid.org/0000-0002-9124-5155>
- A. Collareta  <http://orcid.org/0000-0002-6513-8882>
- K. Gariboldi  <http://orcid.org/0000-0002-7978-7496>
- A. Gioncada  <http://orcid.org/0000-0002-8513-7377>
- D. Jablonska  <http://orcid.org/0000-0002-5055-3282>
- W. Landini  <http://orcid.org/0000-0001-7196-9888>
- M. Urbina  <http://orcid.org/0000-0002-1898-9051>
- G. Bianucci  <http://orcid.org/000-0001-7105-0863>

References

- Alván, A., Ramírez, K., von Eynatten, H., Dunkl, I., Jacay, J., & Bertone, G. (2017). Evolución geológica de las cuencas de antearco del sur de Perú (moquegua y camaná-mollendo): proveniencia sedimentaria y análisis de facies en rocas cenozoicas. *Boletín de la Sociedad Geológica del Perú*, 112, 53–77.
- Andjić, G., Baumgartner-Mora, C., Baumgartner, P. O., & Petrizzo, M. R. (2018). Tectono-stratigraphic response of the sandino forearc basin (N-Costa Rica and W-Nicaragua) to episodes of rough crust and oblique subduction. *The Depositional Record*, 4(1), 90–132. <https://doi.org/10.1002/dep2.40>
- Belia, E. R., Nick, K. E., Bedoya Agudelo, E., & Watkins, D. K. (2019). Earliest Miocene calcareous nannofossil biostratigraphy from the low-latitude Pisco Basin (Peru). *Stratigraphy*, 16(2), 87–105. <https://doi.org/10.29041/strat.16.2.87-105>
- Bianucci, G., Bosio, G., Malinverno, E., de Muizon, C., Villa, I. M., Urbina, M., & Lambert, O. (2018a). A new large squalodelphinid (cetacea, Odontoceti) from Peru sheds light on the early miocene platanistoid disparity and ecology. *Royal Society Open Science*, 5(4), Article# 172302. <https://doi.org/10.1098/rsos.172302>
- Bianucci, G., Collareta, A., Bosio, G., Landini, W., Gariboldi, K., Gioncada, A., Lambert, O., Malinverno, E., Muizon, C. d., Varas-Malca, R., Villa, I. M., Coletti, G., Urbina, M., & Di Celma, C. (2018b). Taphonomy and palaeoecology of the lower Miocene marine vertebrate assemblage of Ullujaya (Chilcatay Formation, East Pisco basin, southern Peru). *Palaeogeography, Palaeoclimatology, Palaeoecology*, 511, 256–279. <https://doi.org/10.1016/j.palaeo.2018.08.013>
- Bianucci, G., Di Celma, C., Collareta, A., Landini, W., Post, K., Tinelli, C., de Muizon, C., Bosio, G., Gariboldi, K., Gioncada, A., Malinverno, E., Cantalamessa, G., Altamirano-Sierra, A., Salas-Gismondi, R., Urbina, M., & Lambert, O. (2016a). Fossil marine vertebrates of Cerro Los quesos: Distribution of cetaceans, seals, crocodiles, seabirds, sharks, and bony fish in a late Miocene locality of the Pisco Basin, Peru. *Journal of Maps*, 12(5), 1037–1046. <https://doi.org/10.1080/17445647.2015.1115785>
- Bianucci, G., Di Celma, C., Landini, W., Post, K., Tinelli, C., Muizon, C. d., Gariboldi, K., Malinverno, E., Cantalamessa, G., Gioncada, A., Collareta, A., Salas-Gismondi, R., Varas-Malca, R. M., Urbina, M., & Lambert, O. (2016b). Distribution of fossil marine vertebrates in Cerro Colorado, the type locality of the giant raptorial sperm whale *livyatan melvillei* (miocene, Pisco Formation, Peru). *Journal of Maps*, 12(3), 543–557. <https://doi.org/10.1080/17445647.2015.1048315>
- Bianucci, G., Di Celma, C., Urbina, M., & Lambert, O. (2016c). New beaked whales from the late Miocene of Peru and evidence for convergent evolution in stem and crown ziphiidae (cetacea, odontoceti). *PeerJ*, 4, article# e2479. <https://doi.org/10.7717/peerj.2479>
- Bosio, G., Bracchi, A. V., Malinverno, E., Collareta, A., Coletti, G., Gioncada, A., Kočí, T., Di Celma, C., Bianucci, G., & Basso, D. (2021a). Taphonomy of a *panopea ménard de la groye*, 1807 shell bed from the Pisco Formation (miocene, Peru). *Comptes Rendus Palevol*, 20 (8), 119–140. <https://doi.org/10.5852/cr-palevol2021.20.5852>
- Bosio, G., Collareta, A., Di Celma, C., Lambert, O., Marx, F. G., de Muizon, C., Gioncada, A., Gariboldi, K., Malinverno, E., Varas Malca, R., Urbina, M., &

- Bianucci, G. (2021b). Taphonomy of marine vertebrates of the Pisco Formation (miocene, Peru): insights into the origin of an outstanding konzentrat- and konservat-lagerstätte. *PLoS ONE*, 16(7), article# e0254395. <https://doi.org/10.1371/journal.pone.0254395>
- Bosio, G., Gioncada, A., Di Celma, C., Villa, I. M., Pichavant, M., Urbina, M., & Bianucci, G. (2020a). Two-mica rhyolitic tephra in the East Pisco Basin (Peru): new age and dispersion constraints for the eruptions of the Eastern Cordillera of central Andes. *Bulletin of Volcanology*, 82(6), article #43. <https://doi.org/10.1007/s00445-020-1373-y>
- Bosio, G., Gioncada, A., Malinverno, E., Di Celma, C., Villa, I. M., Cataldi, G., Gariboldi, K., Collareta, A., Urbina, M., & Bianucci, G. (2019). Chemical and petrographic fingerprinting of volcanic ashes as a tool for high-resolution stratigraphy of the upper Miocene Pisco Formation (Peru). *Journal of the Geological Society, London*, 176(1), 13–28. <https://doi.org/10.1144/jgs2018-071>
- Bosio, G., Malinverno, E., Collareta, A., Di Celma, C., Gioncada, A., Parente, M., Berra, F., Marx, F. G., Vertino, A., Urbina, M., & Bianucci, G. (2020b). Strontium isotope stratigraphy and the thermophilic fossil fauna from the middle Miocene of the East Pisco Basin (Peru). *Journal of South American Earth Sciences*, 97, article #102399. <https://doi.org/10.1016/j.jsames.2019.102399>
- Bosio, G., Malinverno, E., Villa, I. M., Di Celma, C., Gariboldi, K., Gioncada, A., Barberini, V., Urbina, M., & Bianucci, G. (2020c). Tephrochronology and chronostratigraphy of the Miocene Chilcatay and Pisco formations (East Pisco Basin, Peru). *Newsletters on Stratigraphy*, 53(2), 213–247. <https://doi.org/10.1127/nos/2019/0525>
- Brand, L., Urbina, M., Chadwick, A., DeVries, J. T., & Esperante, R. (2011). A high-resolution stratigraphic framework for the remarkable fossil cetacean assemblage of the miocene-Pliocene Pisco Formation, Peru. *Journal of South American Earth Sciences*, 31(4), 414–425. <https://doi.org/10.1016/j.jsames.2011.02.015>
- Carmona, N. B., Mángano, M. G., Buatois, L. A., & Ponce, J. (2007). Bivalve trace fossils in an early Miocene discontinuity surface in patagonia, Argentina: Burrowing behavior and implications for ichnotaxonomy at the firmground-hardground divide. *Palaeogeography, Palaeoclimatology, Palaeoecology*, 255(3-4), 329–341. <https://doi.org/10.1016/j.palaeo.2007.07.014>
- Catuneanu, O., Abreu, V., Bhattacharya, J. P., Blum, M. D., Dalrymple, R. W., Eriksson, P. G., Fielding, C. R., Fisher, W. L., Galloway, W. E., Gibling, M. R., Giles, K. A., Holbrook, J. M., Jordan, R., Kendall, C. G. S. C., Macurda, B., Martinsen, O. J., Miall, A. D., Neal, J. E., Nummedal, D., ... Winker, C. (2019). Towards the standardization of sequence stratigraphy. *Earth-Science Reviews*, 92(1-2), 1–33. <https://doi.org/10.1016/j.earscirev.2008.10.003>
- Clift, P. D., & Hartley, A. J. (2007). Slow rates of subduction erosion and coastal underplating along the Andean margin of Chile and Peru. *Geology*, 35(6), 503–506. <https://doi.org/10.1130/G23584A.1>
- Clift, P. D., Pecker, I., Kukowski, N., & Hampel, A. (2003). Tectonic erosion of the Peruvian forearc, Lima basin, by subduction and Nazca Ridge collision. *Tectonics*, 22(3), 1023. <https://doi.org/10.1029/2002TC001386>
- Coletti, G., Bosio, G., Collareta, A., Malinverno, E., Bracchi, V., Di Celma, C., Basso, D., Stainbank, S., Spezzaferri, S., Cannings, T., & Bianucci, G. (2019). Biostratigraphic, evolutionary, and paleoenvironmental significance of the southernmost lepidocylinids of the Pacific coast of South America (East Pisco Basin, southern Peru). *Journal of South American Earth Sciences*, 96, article #102372. <https://doi.org/10.1016/j.jsames.2019.102372>
- Collareta, A., Di Celma, C., Bosio, G., Pierantoni, P. P., Malinverno, E., Lambert, O., Marx, F. G., Landini, W., Urbina, M., & Bianucci, G. (2021a). Distribution and paleoenvironmental framework of middle Miocene marine vertebrates along the western side of the lower Ica Valley (East Pisco Basin, Peru). *Journal of Maps*, 17(2), 7–17. <https://doi.org/10.1080/17445647.2020.1850535>
- Collareta, A., Lambert, O., Marx, F. G., Muizon, C. d., Varas-Malca, R., Landini, W., Bosio, G., Malinverno, E., Gariboldi, K., Gioncada, A., Urbina, M., & Bianucci, G. (2021b). Vertebrate Palaeoecology of the Pisco Formation (miocene, Peru): glimpses into the ancient humboldt Current ecosystem. *Journal of Marine Science and Engineering*, 9(11), article #1188. <https://doi.org/10.3390/jmse9111188>
- DeVries, T. J. (1998). Oligocene deposition and Cenozoic sequence boundaries in the Pisco Basin (Peru). *Journal of South American Earth Sciences*, 11(3), 217–231. [https://doi.org/10.1016/S0895-9811\(98\)00014-5](https://doi.org/10.1016/S0895-9811(98)00014-5)
- DeVries, T. J. (2016). Fossil Cenozoic crassatelline bivalves from Peru: New species and generic insights. *Acta Palaeontologica Polonica*, 61, 661–688. <https://doi.org/10.4202/app.00228.2015>
- DeVries, T. J. (2017). Eocene stratigraphy and depositional history near puerto Caballas (East Pisco Basin, Peru). *Boletín de la Sociedad Geológica del Perú*, 112, 39–52.
- DeVries, T. J. (2019). Early Paleogene brackish-water molluscs from the Caballas Formation of the East Pisco Basin (southern Peru). *Journal of Natural History*, 53 (25–26), 1533–1584. <https://doi.org/10.1080/00222933.2018.1524032>
- DeVries, T. J., Barron, J. A., Urbina-Schmitt, M., Ochoa, D., Esperante, R., & Snee, L. W. (2021). The Miocene stratigraphy of the Laberinto area (Río Ica Valley) and its bearing on the geological history of the East Pisco Basin (south-central Peru). *Journal of South American Earth Sciences*, 111, article #103458. <https://doi.org/10.1016/j.jsames.2021.103458>
- DeVries, T. J., & Jud, N. A. (2018). Lithofacies patterns and paleogeography of the Miocene Chilcatay and lower Pisco depositional sequences (East Pisco Basin, Peru). *Boletín de la Sociedad Geológica del Perú, Volumen Jubilar*, 8, 124–167.
- DeVries, T. J., & Schrader, H. (1997). Middle Miocene marine sediments in the Pisco basin (Peru). *Boletín de la Sociedad Geológica del Perú*, 87, 1–13.
- DeVries, T. J., Urbina, M., & Jud, N. A. (2017). The Eocene-Oligocene Otuma depositional sequence (East Pisco Basin, Peru): paleogeographic and paleoceanographic implications of new data. *Boletín de la Sociedad Geológica del Perú*, 112, 14–38.
- Di Celma, C., & Cantalamessa, G. (2007). Sedimentology and high-frequency sequence stratigraphy of a forearc extensional basin: The Miocene caleta herradura formation, mejillones peninsula, northern Chile. *Sedimentary Geology*, 198(1-2), 29–52. <https://doi.org/10.1016/j.sedgeo.2006.11.003>
- Di Celma, C., Malinverno, E., Bosio, G., Collareta, A., Gariboldi, K., Gioncada, A., Molli, G., Basso, D., Varas-Malca, R., Pierantoni, P. P., Villa, I. M., Lambert, O., Landini, W., Sarti, G., Cantalamessa, G., Urbina, M., & Bianucci, G. (2017). Sequence stratigraphy and

- paleontology of the upper Miocene Pisco Formation along the western side of the lower Ica Valley (Ica Desert, Peru). *Rivista Italiana di Paleontologia e Stratigrafia (Research in Paleontology and Stratigraphy)*, 123(2), 255–273. <https://doi.org/10.13130/2039-4942/8373>.
- Di Celma, C., Malinverno, E., Bosio, G., Gariboldi, K., Collareta, A., Gioncada, A., Landini, W., Pierantoni, P. P., & Bianucci, G. (2018a). Intraformational unconformities as a record of late Miocene eustatic falls of sea level in the Pisco Formation (southern Peru). *Journal of Maps*, 14 (2), 607–619. <https://doi.org/10.1080/17445647.2018.1517701>
- Di Celma, C., Malinverno, E., Cantalamessa, G., Gioncada, A., Bosio, G., Villa, I. M., Gariboldi, K., Rustichelli, A., Pierantoni, P. P., Landini, W., Tinelli, C., Collareta, A., & Bianucci, G. (2016a). Stratigraphic framework of the late Miocene Pisco Formation at Cerro Los Quesos (Ica Desert, Peru). *Journal of Maps*, 12(5), 1020–1028. <https://doi.org/10.1080/17445647.2015.1115783>
- Di Celma, C., Malinverno, E., Collareta, A., Bosio, G., Gariboldi, K., Lambert, O., Landini, W., Pierantoni, P. P., Gioncada, A., Villa, I. M., Coletti, G., Muizon, C. d., Urbina, M., & Bianucci, G. (2018b). Facies analysis, stratigraphy and marine vertebrate assemblage of the lower Miocene Chilcatay Formation at Ullujaya (Pisco Basin, Peru). *Journal of Maps*, 14(2), 257–268. <https://doi.org/10.1080/17445647.2018.1456490>
- Di Celma, C., Malinverno, E., Gariboldi, K., Gioncada, A., Rustichelli, A., Pierantoni, P. P., Landini, W., Bosio, G., Tinelli, C., & Bianucci, G. (2016b). Stratigraphic framework of the late Miocene to Pliocene Pisco formation at Cerro Colorado (Ica Desert, Peru). *Journal of Maps*, 12 (3), 515–529. <https://doi.org/10.1080/17445647.2015.1047906>
- Di Celma, C., Pierantoni, P. P., Malinverno, E., Collareta, A., Lambert, O., Landini, W., Bosio, G., Gariboldi, K., Gioncada, A., de Muizon, C., Molli, G., Marx, F. G., Varas-Malca, R. M., Urbina, M., & Bianucci, G. (2019). Allostratigraphy and paleontology of the lower Miocene Chilcatay Formation in the Zamaca area, East Pisco basin, southern Peru. *Journal of Maps*, 15(2), 393–405. <https://doi.org/10.1080/17445647.2019.1604439>
- Draut, A. E., & Clift, P. D. (2013). Differential preservation in the geologic record of intraoceanic arc sedimentary and tectonic processes. *Earth-Science Reviews*, 116, 57–84. <https://doi.org/10.1016/j.earscirev.2012.11.003>
- Dunbar, R. B., Marty, R. C., & Baker, P. A. (1990). Cenozoic marine sedimentation in the secura and Pisco basins, Peru. *Palaeogeography, Palaeoclimatology, Palaeoecology*, 77(3-4), 235–261. [https://doi.org/10.1016/0031-0182\(90\)90179-B](https://doi.org/10.1016/0031-0182(90)90179-B)
- Esperante, R., Brand, L. R., Chadwick, A. V., & Poma, O. (2015). Taphonomy and paleoenvironmental conditions of deposition of fossil whales in the diatomaceous sediments of the miocene/Pliocene Pisco Formation, southern Peru—A new fossil-lagerstätte. *Palaeogeography, Palaeoclimatology, Palaeoecology*, 417, 337–370. <https://doi.org/10.1016/j.palaeo.2014.09.029>
- Gariboldi, K., Bosio, G., Malinverno, E., Gioncada, A., Di Celma, C., Villa, I. M., Urbina, M., & Bianucci, G. (2017). Biostratigraphy, geochronology and sedimentation rates of the upper Miocene Pisco Formation at two important marine vertebrate fossil-bearing sites of southern Peru. *Newsletters on Stratigraphy*, 50(4), 417–444. <https://doi.org/10.1127/nos/2017/0345>
- Gariboldi, K., Gioncada, A., Bosio, G., Malinverno, E., Di Celma, C., Tinelli, C., Urbina, M., & Bianucci, G. (2015). The dolomite nodules enclosing fossil marine vertebrates in the East Pisco Basin, Peru: Field and petrographic insights into the Lagerstätte formation. *Palaeogeography, Palaeoclimatology, Palaeoecology*, 438, 81–95. <https://doi.org/10.1016/j.palaeo.2015.07.047>
- Genge, M. C., Witt, C., Chanier, F., Reynaud, J.-Y., & Calderon, Y. (2020). Outer forearc high control in an erosional subduction regime: The case of the central Peruvian forearc (6–10°S). *Tectonophysics*, 789, article #228546. <https://doi.org/10.1016/j.tecto.2020.228546>
- Gioncada, A., Collareta, A., Gariboldi, K., Lambert, O., Di Celma, C., Bonaccorsi, E., Urbina, M., & Bianucci, G. (2016). Inside baleen: Exceptional microstructure preservation in a late Miocene whale skeleton from Peru. *Geology*, 44(10), 839–842. <https://doi.org/10.1130/G38216.1>
- Gioncada, A., Gariboldi, K., Collareta, A., Di Celma, C., Bosio, G., Malinverno, E., Lambert, O., Pike, J., Urbina, M., & Bianucci, G. (2018a). Looking for the key to preservation of fossil marine vertebrates in the Pisco Formation of Peru: New insights from a small dolphin skeleton. *Andean Geology*, 45(3), 379–398. <https://doi.org/10.5027/andgeoV45n3-3122>
- Gioncada, A., Petrini, R., Bosio, G., Gariboldi, K., Collareta, A., Malinverno, E., Bonaccorsi, E., Di Celma, C., Pasero, M., Urbina, M., & Bianucci, G. (2018b). Insights into the diagenetic environment of fossil marine vertebrates of the Pisco Formation (late miocene, Peru) from mineralogical and Sr-isotope data. *Journal of South American Earth Sciences*, 81, 141–152. <https://doi.org/10.1016/j.jsames.2017.11.014>
- Hagen, R. A., & Moberly, R. (1994). Tectonic effects of a subducting aseismic ridge: The subduction of the Nazca Ridge at the Peru trench. *Marine Geophysical Researches*, 16(2), 145–161. <https://doi.org/10.1007/BF01224757>
- Hampel, A. (2002). The migration history of the Nazca Ridge along the Peruvian active margin: A re-evaluation. *Earth and Planetary Science Letters*, 203(2), 665–679. [https://doi.org/10.1016/S0012-821X\(02\)00859-2](https://doi.org/10.1016/S0012-821X(02)00859-2)
- Herbozo, G., Kukowski, N., Clift, P. D., Pecker, I., & Bolaños, R. (2020). Cenozoic increase in subduction erosion during plate convergence variability along the convergent margin off Trujillo, Peru. *Tectonophysics*, 790, article #228557. <https://doi.org/10.1016/j.tecto.2020.228557>
- Hernández, M. J., Michaud, F., Collot, J.-Y., Proust, J.-N., & d'Acremont, E. (2020). Evolution of the Ecuador offshore nonaccretionary-type forearc basin and margin segmentation. *Tectonophysics*, 781, article #228374. <https://doi.org/10.1016/j.tecto.2020.228374>
- Hernández-Molina, F. J., Fernández-Salas, L. M., Lobo, F., Somoza, L., Díaz-del-Río, V., & Alveirinho Dias, J. M. (2000). The infralittoral prograding wedge: A new large-scale progradational sedimentary body in shallow marine environments. *Geo-Marine Letters*, 20(2), 109–117. <https://doi.org/10.1007/s003670000040>
- Hsu, J. T. (1992). Quaternary uplift of the Peruvian coast related to the subduction of the Nazca Ridge: 13.5 to 15.6 degrees south latitude. *Quaternary International*, 15, 87–97. [https://doi.org/10.1016/1040-6182\(92\)90038-4](https://doi.org/10.1016/1040-6182(92)90038-4)
- Kent, B. A. P., Dashtgard, S. E., Huang, C., MacEachern, J. A., Gibson, H. D., & Cathyl-Huhn, G. (2020). Initiation and early evolution of a forearc basin: Georgia basin.

- Canada. Basin Research*, 32(1), 163–185. <https://doi.org/10.1111/bre.12378>
- Kočí, T., Bosio, G., Collareta, A., Sanfilippo, R., Ekrt, B., Urbina, M., & Malinverno, E. (2021). First record of cirratulid (annelida, polychaeta) reefs from the Miocene Chilcatay and Pisco formations (East Pisco basin, Peru). *Journal of South American Earth Sciences*, 107, article #103042. <https://doi.org/10.1016/j.jsames.2020.103042>
- Kulm, L. D., Resig, J. M., Thornburg, T. M., & Schrader, H. J. (1982). Cenozoic structure, stratigraphy and tectonics of the central Peru forearc. In J. K. Legget (Ed.), *Trench and forearc geology: Sedimentation and tectonics on modern and ancient plate margins* (pp. 151–169). Blackwells. <https://doi.org/10.1144/GSL.SP.1982.010.01.10>
- Lambert, O., Bianucci, G., Salas-Gismondi, R., Di Celma, C., Steurbaut, E., Urbina, M., & de Muizon, C. (2019). An amphibious whale from the middle Eocene of Peru reveals early south Pacific dispersal of quadrupedal cetaceans. *Current Biology*, 29(8), 1352–1359. <https://doi.org/10.1016/j.cub.2019.02.050>
- Lambert, O., Collareta, A., Benites-Palombino, A., Di Celma, C., de Muizon, C., & Bianucci, G. (2021). A new small, mesorostrine inioid (cetacea, odontoceti, delphinida) from late Miocene localities of the Pisco Basin, Peru. *Papers in Palaeontology*, 7(2), 1043–1064. <https://doi.org/10.1002/spp.2.1332>
- Lambert, O., de Muizon, C., Malinverno, E., Di Celma, C., Urbina, M., & Bianucci, G. (2018). A new odontocete (toothed cetacean) from the early Miocene of Peru expands the morphological disparity of extinct heterodont dolphins. *Journal of Systematic Palaeontology*, 16(12), 981–1016. <https://doi.org/10.1080/14772019.2017.1359689>
- Lambert, O., de Muizon, C., Urbina, M., & Bianucci, G. (2020). A new longirostrine sperm whale (cetacea, physeteroidea) from the lower Miocene of the Pisco Basin (southern coast of Peru). *Journal of Systematic Palaeontology*, 18(20), 1707–1742. <https://doi.org/10.1080/14772019.2020.1805520>
- Lambert, O., Martínez-Cáceres, M., Bianucci, G., Di Celma, C., Salas-Gismondi, R., Steurbaut, E., Urbina, M., & de Muizon, C. (2017). Earliest mysticete from the late Eocene of Peru sheds new light on the origin of baleen whales. *Current Biology*, 27(10), 1535–1541. <https://doi.org/10.1016/j.cub.2017.04.026>
- Landini, W., Altamirano-Sierra, A., Collareta, A., Di Celma, C., Urbina, M., & Bianucci, G. (2017a). The late Miocene elasmobranch assemblage from Cerro Colorado (Pisco Formation, Peru). *Journal of South American Earth Sciences*, 73, 168–190. <https://doi.org/10.1016/j.jsames.2016.12.010>
- Landini, W., Collareta, A., Di Celma, C., Malinverno, E., Urbina, M., & Bianucci, G. (2019). The early Miocene elasmobranch assemblage from Zamaca (Chilcatay Formation, Peru). *Journal of South American Earth Sciences*, 91, 352–371. <https://doi.org/10.1016/j.jsames.2018.08.004>
- Landini, W., Collareta, A., Pesci, F., Di Celma, C., Urbina, M., & Bianucci, G. (2017b). A secondary nursery area for the copper shark *carcharhinus brachyurus* from the late Miocene of Peru. *Journal of South American Earth Sciences*, 78, 164–174. <https://doi.org/10.1016/j.jsames.2017.07.003>
- León, W., Aleman, A., Torres, V., Rosell, W., & De La Cruz, O. (2008). Estratigrafía, sedimentología y evolución tectónica de la cuenca Pisco oriental. *Boletín INGEMMET*, 27(Serie D), 144. Lima, Peru.
- MacEachern, J. A., Raychaudhuri, I., & Pemberton, S. G. (1992). Stratigraphic applications of the Glossifungites ichnofacies: Delineating discontinuities in the rock record. In S. G. Pemberton (Ed.), *Application of ichnology to petroleum exploration, a core workshop*. SEPM Core workshop no. 17 (pp. 169–198). SEPM. <https://doi.org/10.2110/cor.92.01.0169>.
- Macharé, J., & Ortlieb, L. (1992). Plio-Quaternary vertical motions and the subduction of the Nazca Ridge, central coast of Peru. *Tectonophysics*, 205(1-3), 97–108. [https://doi.org/10.1016/0040-1951\(92\)90420-B](https://doi.org/10.1016/0040-1951(92)90420-B)
- Malinverno, E., Bosio, G., Di Celma, C., Gariboldi, K., Gioncada, A., Pierantoni, P. P., Collareta, A., Molli, G., Bagnoli, G., Sarti, G., Urbina, M., & Bianucci, G. (2021). (Bio)stratigraphic overview and paleoclimatic-paleoceanographic implications of the middle-upper Eocene deposits from the Ica River Valley (East Pisco Basin, Peru). *Palaeogeography, Palaeoclimatology, Palaeoecology*, 578, article #11056. <https://doi.org/10.1016/j.palaeo.2021.110567>
- Marx, F. G., Collareta, A., Gioncada, A., Post, K., Lambert, O., Bonaccorsi, E., Urbina, M., & Bianucci, G. (2017a). How whales used to filter: Exceptionally preserved baleen in a Miocene cetotheriid. *Journal of Anatomy*, 231(2), 212–220. <https://doi.org/10.1111/joa.12622>
- Marx, F. G., Lambert, O., & de Muizon, C. (2017b). A new Miocene baleen whale from Peru deciphers the Dawn of cetotheriids. *Royal Society Open Science*, 4(9), article #170560. <https://doi.org/10.1098/rsos.170560>
- McNeill, L. C., Goldfinger, C., Kulm, L. D., & Yeats, R. S. (2000). Tectonics of the Neogene Cascadia forearc basin: Investigations of a deformed late Miocene unconformity. *Geological Society of America Bulletin*, 112(8), 1209–1224. [https://doi.org/10.1130/0016-7606\(2000\)112<1209:TOTNCF>2.0.CO;2](https://doi.org/10.1130/0016-7606(2000)112<1209:TOTNCF>2.0.CO;2)
- Mukasa, S. B., & Henry, D. J. (1990). The San Nicolas Batholith of coastal Peru: Early Paleozoic continental arc or continental rift magmatism. *Journal of the Geological Society, London*, 147(1), 27–39. <https://doi.org/10.1144/gsjgs.147.1.0027>
- NACSN (North American Commission on Stratigraphic Nomenclature). (2005). North American stratigraphic code. *American Association of Petroleum Geologists Bulletin*, 89(11), 1547–1591. <https://doi.org/10.1306/07050504129>
- Noda, A. (2016). Forearc basins: Types, geometries, and relationships to subduction zone dynamics. *Geological Society of America Bulletin*, 128(5-6), 879–895. <https://doi.org/10.1130/B31345.1>
- Ochoa, D., Salas-Gismondi, R., DeVries, J. T., Baby, P., de Muizon, C., Altamirano, A., Barbosa-Espitia, A., Foster, D. A., Quispe, K., Cardich, J., Gutiérrez, D., Perez, A., Valqui, J., Urbina, M., & Carré, M. (2021). Late Neogene evolution of the Peruvian margin and its ecosystems: A synthesis from the Sacaco record. *International Journal of Earth Sciences*, 110(3), 995–1025. <https://doi.org/10.1007/s00531-021-02003-1>
- Patruno, S., & Helland Hansen, W. (2018). Clinoforms and clinoform systems: Review and dynamic classification scheme for shorelines, subaqueous deltas, shelf edges and continental margins. *Earth-Science Reviews*, 185, 202–233. <https://doi.org/10.1016/j.earscirev.2018.05.016>
- Pemberton, S. G., MacEachern, J. A., & Saunders, T. (2004). Stratigraphic applications of substrate-specific ichnofacies: Delineating discontinuities in the fossil record. In

- D. McIlroy (Ed.), *The application of ichnology to palaeoenvironmental and stratigraphic analysis. Geological Society of London special publication*, 228 (pp. 29–62). Geological Society of London. <https://doi.org/10.1144/GSL.SP.2004.228.01.03>.
- Phillips, T. B., Jackson, A.-L., & Norcliffe, J. R. (2020). Pre-inversion normal fault geometry controls inversion style and magnitude, farsund basin, offshore southern Norway. *Solid Earth*, 11(4), 1489–1510. <https://doi.org/10.5194/se-11-1489-2020>
- Prudhomme, A., Baby, P., Robert, A., Brichau, S., Cuipa, E., Eude, A., Calderon, Y., & O'Sullivan, P. (2019). Western thrusting and uplift in northern Central Andes (western Peruvian margin). In B. K. Horton, & A. Folguera (Eds.), *Andean tectonics* (pp. 299–331). Elsevier. <https://doi.org/10.1016/B978-0-12-816009-1.00013-7>
- Quispe, K., Baby, P., Calderón, Y., Hurtado, C., & Ramírez, L. (2018). La cuenca Pisco: nuevo modelo estructural para una cuenca de antearco peruana, evidencias de contexto compresivo, desarrollo de la Cordillera de la Costa. *XIX Congreso Peruano de Geología*. <https://doi.org/10.13140/RG.2.2.11140.68483>
- Ramos, V. A. (2008). The basement of the Central Andes: The Arequipa and related terranes. *Annual Review of Earth and Planetary Sciences*, 36(1), 289–324. <https://doi.org/10.1146/annurev.earth.36.031207.124304>
- Romero, D., Valencia, K., Alarcón, P., Peña, D., & Ramos, V. A. (2013). The offshore basement of Peru: Evidence for different igneous and metamorphic domains in the fore-arc. *Journal of South American Earth Sciences*, 42, 47–60. <https://doi.org/10.1016/j.jsames.2012.11.003>
- Rustichelli, A., Di Celma, C., Tondi, E., Baud, P., & Vinciguerra, S. (2016a). Fibrous gypsum veins as diffuse features and within fault zones: The case study of the Pisco Basin (Ica desert, southern Peru). *Journal of the Geological Society, London*, 173(3), 405–418. <https://doi.org/10.1144/jgs2015-084>
- Rustichelli, A., Di Celma, C., Tondi, E., & Bianucci, G. (2016b). Deformation within the Pisco basin sedimentary record (southern Peru): stratabound orthogonal vein sets and their impact on fault development. *Journal of South American Earth Sciences*, 65, 79–100. <https://doi.org/10.1016/j.jsames.2015.11.002>
- Sanfilippo, R., Kočí, T., Bosio, G., Collareta, A., Ekrt, B., Malinverno, E., Di Celma, C., Urbina, M., & Bianucci, G. (2021). An investigation of vermetid reefs from the Miocene of Peru, with the description of a new species. *Journal of South American Earth Sciences*, 108, article #103233. <https://doi.org/10.1016/j.jsames.2021.103233>
- Sébrier, M., Lavenu, A., Fornari, M., & Soulard, J.-P. (1988). Tectonics and uplift in the Central Andes (Peru, Bolivia and northern Chile) from Eocene to present. *Geodynamique*, 3(1-2), 85–106.
- Stucchi, M., Varas-Malca, R. M., & Urbina-Schmitt, M. (2016). New Miocene sulid birds from Peru and considerations on their Neogene fossil record in the eastern Pacific Ocean. *Acta Palaeontologica Polonica*, 61(2), 417–427. <http://doi.org/10.4202/app.00170.2015>
- Thornburg, T. M., & Kulm, L. D. (1981). Sedimentary basins of the Peru continental margin: Structure, stratigraphy, and Cenozoic tectonics from 6°S to 16°S latitude. In L. D. Kulm, J. Dymond, E. J. Dasch, & D. M. Hussong (Eds.), *Nazca plate: Crustal formation and Andean convergence. Geological Society of America, Memoir 154* (pp. 393–422). Geological Society of America.
- Timoteo, D., Junior, F. C., & Borda, E. (2017). Application of seismic stratigraphy for frontier Hydrocarbon exploration, Salaverry basin, Peru: Insights into potential reservoirs. *Boletín de La Sociedad Geológica Del Perú*, 112, 103–128.
- Travis, R. B., Gonzales, G., & Pardo, A. (1976). Hydrocarbon potential of coastal basins of Peru. *AAPG Memoir*, 25, 331–338. <https://doi.org/10.1306/83D918CB-16C7-11D7-8645000102C1865D>
- Viveen, W., & Schlunegger, F. (2018). Prolonged extension and subsidence of the Peruvian forearc during the cenozoic. *Tectonophysics*, 730, 48–62. <https://doi.org/10.1016/j.tecto.2018.02.018>
- von Huene, R., & Lallemand, S. (1990). Tectonic erosion along the Japan and Peru convergent margins. *Geological Society of America Bulletin*, 102(6), 704–720. [https://doi.org/10.1130/0016-7606\(1990\)102<0704:TEATJA>2.3.CO;2](https://doi.org/10.1130/0016-7606(1990)102<0704:TEATJA>2.3.CO;2)
- Witt, C., Reynaud, J. Y., Barba, D., Poujol, M., Aizprua, C., Rivadeneira, M., & Amberg, C. (2019). From accretion to forearc basin initiation: The case of SW Ecuador, northern Andes. *Sedimentary Geology*, 379, 138–157. <https://doi.org/10.1016/j.sedgeo.2018.11.009>
- Wright, R., Dunbar, R. B., Allen, M., & Baker, P. (1989). Morphology of stacked marine delta lobes, East Pisco Basin, Peru. In A. W. Bally (Ed.), *Atlas of seismic stratigraphy* (pp. 192–196). AAPG, Studies in Geology, #27, v. III.
- Zecchin, M., Catuneanu, O., & Caffau, M. (2018). Wave-ravinement surfaces: Classification and key characteristics. *Earth-Science Reviews*, 188, 210–239. <https://doi.org/10.1016/j.earscirev.2018.11.011>